Impact of Atmospheric Intraseasonal Oscillations on the Indian Ocean Dipole during the 1990s*

WEIQING HAN
Program in Atmospheric and Oceanic Sciences, University of Colorado, Boulder, Colorado
TOSHIAKI SHINODA
NOAA–Cooperative Institute for Research in Environmental Sciences Climate Diagnostics Center, Boulder, Colorado
LEE-LUENG FU
Jet Propulsion Laboratory, California Institute of Technology, Pasadena, California
JULIAN P. MCCREARY
International Pacific Research Center, University of Hawaii at Manoa, Honolulu, Hawaii

(Manuscript received 1 February 2005, in final form 27 September 2005)

ABSTRACT

Effects of atmospheric intraseasonal oscillations (ISOs) on the Indian Ocean zonal dipole mode (IOZDM) are investigated by analyzing available observations and a suite of solutions to an ocean general circulation model, namely, the Hybrid Coordinate Ocean Model (HYCOM). Data and model solutions for the period 1991–2000 are analyzed, a period that includes two strong IOZDM events, during 1994 and 1997, and a weak one, in 1991. Both the data analysis and model results suggest that atmospheric ISOs play a significant role in causing irregularity of the two strong IOZDM events and the premature termination of the weak one. Of particular interest is a basinwide, wind-driven oceanic resonance with a period near 90 days, involving the propagation of equatorial Kelvin and first-meridional-mode Rossby waves across the basin. Before the onset of the strong 1997 dipole, wind variability had significant power near 90 days, and the resonance was strongly excited. Associated with the resonance was a deepened thermocline in the eastern basin during August and early September, which reduced the upwelling in the eastern antinode region of the IOZDM, thereby delaying the reversal of the equatorial zonal SST gradient—an important indicator of a strong IOZDM—by over a month. A similar deepened thermocline in the eastern basin also contributed to the premature termination of the weak 1991 dipole. During the 1994 IOZDM, the winds had little power near 90 days, and the resonant mode was not prominent. The ISOs influenced the IOZDM through both surface fluxes and thermocline variability. They enhanced warming in the western antinode region during October, the peak phase of the IOZDM, intensifying its strength. During November, strong winds significantly cooled the western and central basin through upwelling and surface fluxes, cooling SST there and contributing to the early and quick termination of the 1994 event.

1. Introduction

Atmospheric intraseasonal oscillations (ISOs) are an important component of tropical climate, impacting the atmosphere and ocean on a wide range of time scales. Pronounced intraseasonal oscillations of winds and convection are observed in the tropical Indian and western Pacific Oceans (e.g., Madden and Julian 1971, 1972; Knutson and Weickmann 1987; Wang and Rui 1990; Hendon and Salby 1996). Many of the ISOs are generated in the Indian Ocean and they can propagate poleward to affect the Asian summer monsoon (Sikka and Gadgil 1980; Yasunari 1981; Krishnamurti and Subramanyam 1982; Webster 1983; Lawrence and Webster 2001), and eastward to the Pacific to impact ENSO (Lau and Chan 1988; McPhaden 1999; Moore and Kleeman 1999; Takayabu et al. 1999; Kessler and Kleeman 2000; Kiladis and Straub 2001).

* School of Ocean and Earth Science and Technology Contribution Number 6665 and International Pacific Research Center Publication Number 349.

Corresponding author address: Weiqing Han, Program in Atmospheric and Oceanic Sciences, University of Colorado, UCB 311, Boulder, CO 80309.
E-mail: whan@enso.colorado.edu

Observational evidence suggests that the ISOs also drive a large-amplitude oceanic response (Reppin et al. 1999; Webster et al. 2002; Masumoto et al. 2005). In the past few years, extensive modeling studies have been conducted to examine the oceanic response in detail (Shinoda and Hendon 1998; Han et al. 2001, 2004; Sengupta et al. 2001; Schouten et al. 2002; Schiller and Godfrey 2003; Senan et al. 2003; Waliser et al. 2003, 2004; Han 2005). Of particular interest for the present study, Han et al. (2001) and Han (2005) used a hierarchy of models to demonstrate that zonal currents and sea level in the equatorial Indian Ocean have a peak response near a period of 90 days, whereas the forcing winds peak at 30–60 days. The shift in peak frequency between the forcing and response results from the preferential excitation of larger-scale, lower-frequency Kelvin and Rossby waves near the 90-day period and from resonant excitation of the second baroclinic mode by the winds. Resonance occurs at period P when the propagation time for an equatorial Kelvin wave to cross the basin and a first-meridional-mode Rossby wave to return is close to a multiple of P; that is,

$$P = \frac{4L}{mc_n}, \tag{1}$$

where L is the width of the basin along the equator, c_n is the Kelvin wave speed of the nth baroclinic mode, and m is an integer (Jensen 1993; Han et al. 1999). With $n = m = 2$, Eq. (1) is satisfied when P is near 90 days (Han et al. 2001; Han 2005).

Power in the zonal winds at the 90-day period may result from the broad spectral band of ISOs (G. Kiladis 2004, personal communication). It may also arise from the semiannual westerly winds along the equator during spring and autumn, which is not a perfect semiannual oscillation and includes contributions from higher-order harmonics (Han et al. 1999). In this paper, we view the 90-day oceanic waves as part of the intraseasonal response.

The Indian Ocean zonal dipole mode (IOZDM), also referred to as the dipole mode and zonal mode, is a coupled ocean–atmosphere phenomenon in the tropical Indian Ocean that occurs at interannual time scales, typically associated with cold SST anomalies (SSTAs) in the southeastern Tropics and warm SSTAs in the western Tropics (Fig. 1; Saji et al. 1999; Webster et al. 1999). Saji et al. (1999) defined a dipole mode index (DMI) for the IOZDM to be the SSTA difference between the tropical western (10°S–10°N, 50°–70°E) and tropical southeastern (10°S–equator, 90°–110°E) Indian Ocean (dotted curve in Fig. 3a below). Then, one criterion for a strong IOZDM event is that DMI exceeds one standard deviation (Saji et al. 1999) and lasts for 3–4 months during late summer and autumn. In this paper, we refer to an event with DMI below one but above one-half standard deviations as a weak dipole. Accordingly, there were three IOZDM events during 1991–2000: strong events in 1994 and 1997, and a weak one in 1991. These three events were also identified to be IOZDMs by Annamalai et al. (2003), based on the coexistence of ocean–atmosphere variables in the southeastern tropical Indian Ocean and anomalous easterly winds over the central equatorial basin.

It is noteworthy that the two strong and long-lasting IOZDMs are associated with reversed zonal SST gradients in the central and eastern equatorial basins, whereas the weak one is not (Figs. 2g, 2h, and 2f), indicating that a reversed equatorial zonal SST gradient may be a good indicator for a strong IOZDM event. This is because Bjerknes feedback is likely an important process in IOZDM dynamics (e.g., Saji et al. 1999; Murtugudde et al. 2000). In fact, the equatorial zonal SST gradient is strongly correlated with zonal winds over the central equatorial basin during the IOZDM peak period (September–November), with a correlation coefficient of 0.81 and significance above 95% level, based on a 44-yr (1958–2001) extended Reynolds reconstructed SST and European Centre for Medium-Range Weather Forecasts (ECMWF) reanalysis (ERA-40) wind dataset (not shown). This strong correlation further indicates that the Bjerknes feedback is important for the IOZDM development. Indeed, the importance of the equatorial zonal SST gradient and its associated atmospheric response in the equatorial Indian Ocean have been suggested by Murtugudde et al. (1998) and Murtugudde and Busalacchi (1999). The anomalous equatorial easterly was used as one of the four important indices to define a strong IOZDM by Annamalai et al. (2003). When the zonal SST gradient reverses along the equator, the eastern Indian Ocean warm pool and convection are shifted to the central and western basin (Fig. 2), marking the development of a strong IOZDM or the beginning of the strong phase of an IOZDM event.

Available observations suggest that ISO and IOZDM events are often linked. During normal years, ISOs typically occur throughout the year, with westerly winds in the central and eastern equatorial regions and convection maxima located in the warm-pool region of the eastern ocean (Figs. 2a,e). During the strong IOZDM years of 1994 and 1997, however, southeasterly winds prevailed in the eastern basin during boreal summer and autumn. These winds produce equatorial

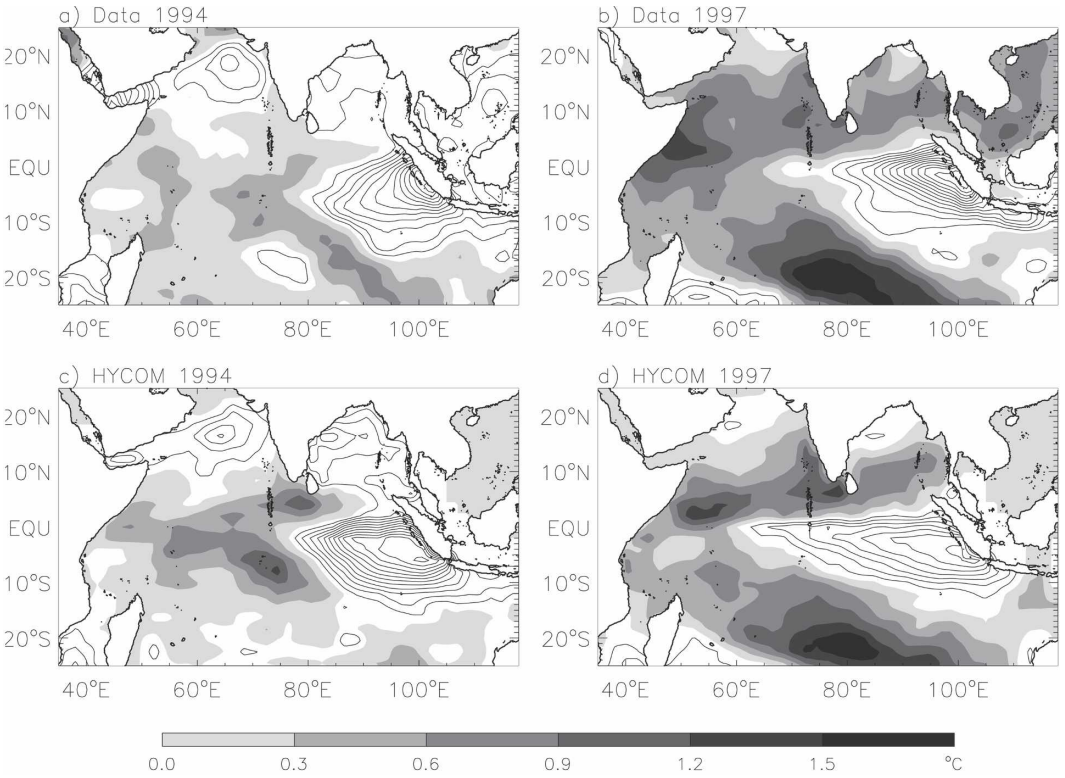

FIG. 1. (a) SSTA during October 1994, the peak of the 1994 dipole. Data are from the NOAA OI weekly SST dataset for the period 1991–2000, a period when the ocean model results are analyzed. To obtain the SSTA, the weekly SST climatology of the 10-yr period is first removed and then the SSTA is averaged over the month. (b) Same as in (a), but for November 1997, when the dipole peaks. (c) Same as in (a), but for the MR solution. (d) Same as in (b), but for the MR solution. Positive values are shaded and negative ones are contoured, with an interval of 0.3°C.

upwelling, reducing the SST and reversing its zonal gradient in the warm-pool region (Figs. 2c, 2d, 2g, and 2h). Corresponding to the westward shifting of the warmest SST, the convection maxima shifted to the western-central basin during 1994 and the western basin during 1997. At the same time, the amplitudes of intraseasonal winds and convection were significantly reduced in the central and eastern basins (Figs. 2c,d; Shinoda and Han 2005). A detailed discussion on how the IOZDMs modify the ISOs is provided by Shinoda and Han (2005).

Differences between individual IOZDM events are also linked to ISOs to a certain degree. For the 1994 event, the reversal of the equatorial zonal SST gradient began in August, reached a peak in October, and quickly terminated in November (Fig. 2g). Coincident with the early termination was a strong ISO event during November (Fig. 2c; Rao and Yamagata 2004). For the 1997 event, equatorial zonal SST-gradient reversal began in September, quickly reached a peak in early October, and continued until January 1998. Coincident with the delayed SST gradient reversal were strong westerly winds associated with ISOs in February, May, and July. During the 1991 weak event, intraseasonal convection and its associated westerly winds frequently occurred during summer and autumn.

The goal of this paper is to understand how atmospheric ISOs affect the onset, development, and termination of the IOZDM. For this purpose, we analyze available data to identify possible impacts, and obtain a suite of solutions to an ocean general circulation model, the Hybrid Coordinate Ocean Model (HYCOM), to identify processes by which ISOs affect the IOZDM SSTA in the eastern and western antinode regions. Note that other processes can also affect the onset and decay of IOZDM events, including processes external to the Indian Ocean that precondition the thermocline depth in the eastern equatorial Indian Ocean (e.g., Annamalai et al. 2005), effects of the seasonal cycle (Halkides 2005), and the Indonesian Throughflow. The scope of this paper, however, is to only examine the effects of the ISOs.

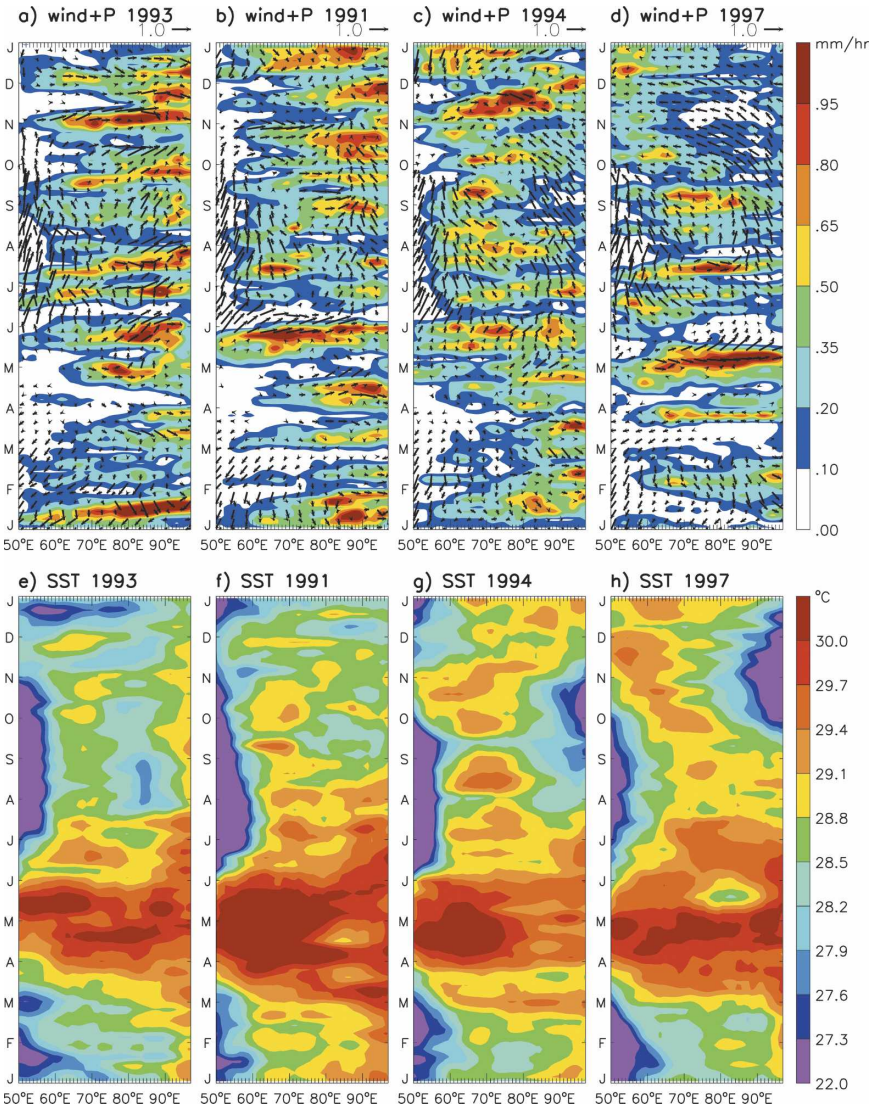

FIG. 2. Longitude–time plots of 3-day-mean ERA-40 surface wind stress (dyn cm^{-2}; arrows) and CMAP pentad precipitation (mm h^{-1}; color contours) averaged over 5°S–5°N of the Indian Ocean during (a) a normal year, 1993, (b) for the weak dipole of 1991, (c) for the strong dipole of 1994, and (d) for the strong dipole of 1997. Longitude–time plots of NOAA OI weekly SST data (°C) averaged over 5°S–5°N of the Indian Ocean during (e) 1993, (f) 1991, (g) 1994, and (h) 1997.

2. Datasets and ocean model

a. Datasets

The datasets we analyze are the ERA-40 3-day-mean surface wind stress for 1991–2000, the period over which the ocean model main solutions will be analyzed; the Climate Prediction Center Merged Analysis of Precipitation (CMAP) pentad data for the same period of time (Xie and Arkin 1996); the Ocean Topography Experiment (TOPEX)/Poseidon 3-day-mean sea level anomaly (SLA) field for 1993–2000 (Fu 2003, 2004); and the National Oceanic and Atmospheric Administration (NOAA) optimum interpolation (OI) weekly SST that includes both in situ and satellite observations for 1991–2000 (Reynolds et al. 2002). To isolate atmospheric ISOs, we apply a Lanczos bandpass filter (Duchon 1979) to the wind stress and precipitation fields, with half-power points at 10 and 105 days. To extract intraseasonal sea level and SST variations, the bandpass filter is applied to the TOPEX/Poseidon SLA and

NOAA OI SST data as well. The SST data are also analyzed to define IOZDM events.

b. Model

Since HYCOM is documented in detail elsewhere (see Bleck 2002), only aspects relevant to this paper are discussed here. HYCOM has a hybrid vertical coordinate that is isopycnal in the open, stratified ocean; terrain-following coordinates in shallow coastal regions; and z coordinates in the mixed layer and unstratified seas. The feasibility of the hybrid coordinate approach for handling both deep and shallow regions throughout the annual heating–cooling cycle has been demonstrated for a North Atlantic basin by Halliwell (1998, 2004).

Our version of HYCOM is configured to the tropical Indian Ocean north of 30°S, with a horizontal resolution of 0.5° × 0.5° and realistic bottom topography (Han et al. 2004; Han 2005). Vertically, 18 sigma layers are chosen with a fine resolution in the upper ocean to better resolve the structures of upper-ocean currents and temperature fields, the thermocline, and the surface mixed layer. Because our focus is on upper-ocean processes, σ_0 is used as a reference pressure. The nonlocal K-profile parameterization is used for the boundary layer mixing scheme (Large et al. 1994, 1997). Shortwave radiation penetration is included with a Jerlov water-type IA (Jerlov 1976).

No-slip conditions are applied along continental boundaries. Near the southern boundary, a sponge layer with a width of 5° (25°–30°S) is applied that relaxes model temperature and salinity fields to the Levitus and Boyer (1994) and Levitus et al. (1994) climatology. Lateral boundary forcing due to the Indonesian Throughflow and Bay of Bengal rivers is included by relaxing the model temperature and salinity to the Levitus data in the corresponding regions. Bottom topographic data are from the 5″ Gridded Earth Topography (ETOPO5) dataset smoothed over a 4° × 4° bin.

The wind stress, wind speed, air temperature, and specific humidity fields used to force the model are taken from the 3-day-mean ERA-40 fields. Net surface shortwave and longwave radiation fields are from 3-day-mean International Satellite Cloud Climatology Project flux data (ISCCP-FD; Zhang et al. 2004). Precipitation is from the CMAP pentad data, interpolated onto the 3-day resolution to be consistent with the ERA-40 and ISCCP forcing fields. These choices are based on a comparison of products. A comparison of ERA-40 and National Aeronautics and Space Administration (NASA) Quick Scatterometer (QuikSCAT) wind stress fields demonstrates that ERA-40 winds are able to reproduce the structure and amplitude of ISOs quite well; furthermore, the ERA-40 winds also agree well with the NASA Scatterometer (NSCAT) winds during 1997. A comparison of precipitation fields in the equatorial Indian Ocean for 1998–2001 from the satellite Tropical Rainfall Measuring Mission (TRMM), CMAP, and the ERA-40 reanalysis shows that CMAP represents the TRMM precipitation field more faithfully than the ERA-40 product. ISCCP shortwave radiation compares favorably with Tropical Ocean and Global Atmosphere Coupled Ocean–Atmosphere Response Experiment (TOGA COARE) shortwave data in the western Pacific.

Table 1 lists the four experiments reported in this paper. For each solution, the model is spun up for 15 yr from a state of rest using monthly climatologies of the above forcing fields. Beginning from year 15, our main run is forced by 3-day-mean fields for the period 1988–2001, so that this solution includes the effects of *all* intraseasonal atmospheric forcing (solution MR). To exclude atmospheric intraseasonal variability entirely, the model is forced over the same period by low-passed fields using a Lanczos filter with a half-power point at 105 days (solution BR). The choice of 105 days ensures that forcing near the 90-day period is removed from solution BR, because at this period the ocean attains a resonant response (section 1). Two test runs are obtained that are like the main run except one is forced by low-passed wind stress only (solution TR1) and the other by low-passed wind stress as well as wind speed (solution TR2), both for the period 1993–99.

We chose the 1988–2001 period for the HYCOM integrations because all the forcing fields are available for that period. Moreover, it includes the 1994 and 1997 strong dipole events, the 1991 weak dipole, and covers the TOPEX/Poseidon observational period. Results for years 1991–2000 are analyzed, considering that transient effects might be included in the first a few years.

c. Validation

As illustrated in Fig. 1, the observed 1994 and 1997 IOZDM events (top panels) are well reproduced by solution MR (bottom panels), with the SSTA fields agreeing in both spatial structure and amplitude. To

TABLE 1. HYCOM experiments. See text for detailed description.

Experiment	Forcing	Duration
MR	3-day mean	1988–2001
BR	Low-passed 105 days	1988–2001
TR1	Low-passed wind stress	1993–99
TR2	Low-passed wind stress and speed	1993–99

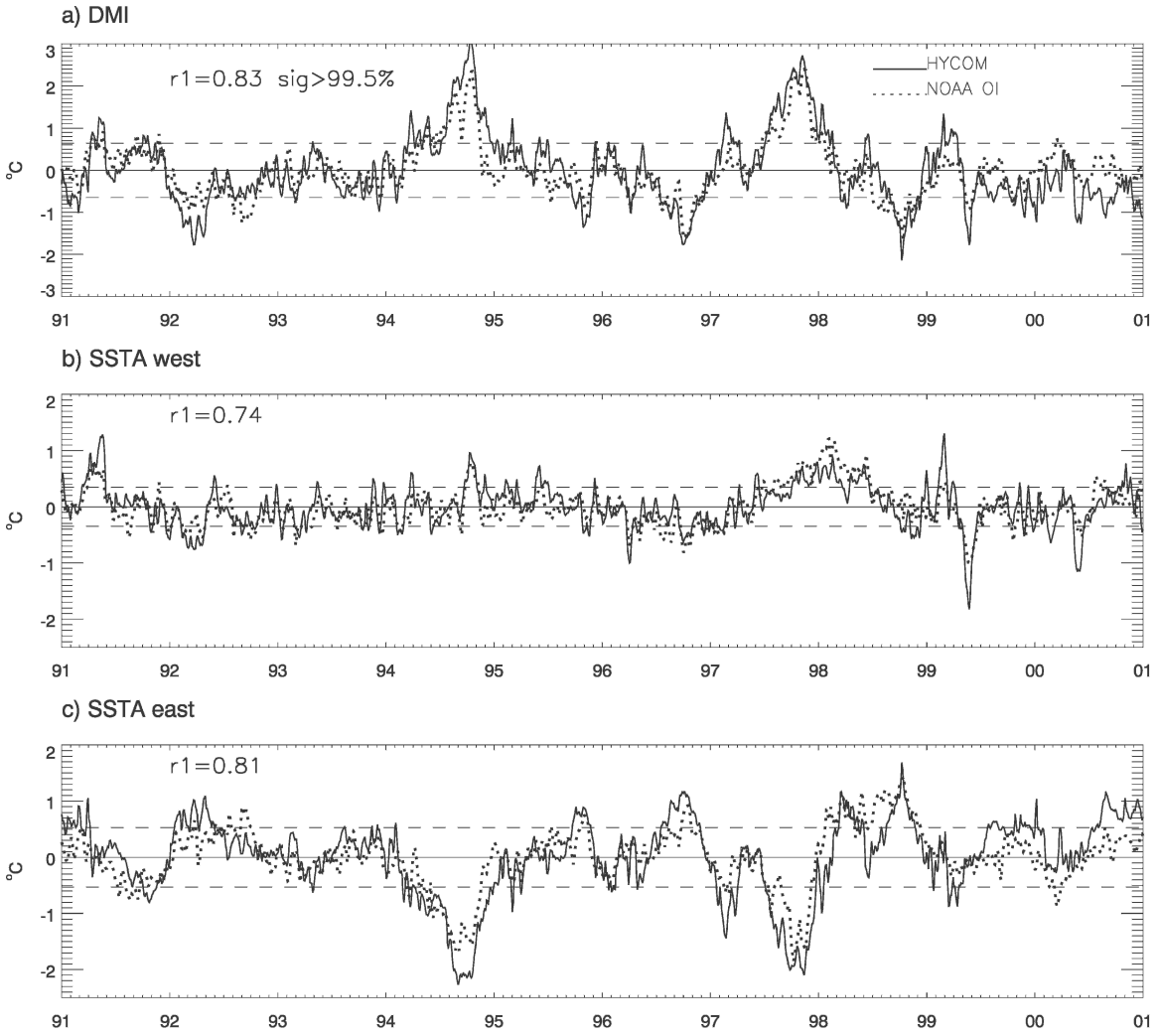

FIG. 3. (a) Time series of observed (dashed curves) and modeled (solid curves) DMI during 1991–2000. The observed data are from the NOAA OI weekly SST data, and the model SST are based on the 3-day-mean MR solution. The 10-yr weekly (3-day mean) climatologies are removed from the observations (model). The two horizontal dashed lines are the one standard deviation value of the observed DMI. (b) Same as in (a), but for the SSTA averaged over the western antinode region (10°S–10°N, 50°–70°E). (c) Same as in (a), but for the SSTA averaged over the eastern antinode region (10°S–0°, 90°–110°E). The DMI shown in (a) is defined as the difference between the SSTA in the western and eastern antinode regions.

quantify how well the MR simulates the SST variability at intraseasonal-to-interannual time scales, Fig. 3 plots time series of observed (dashed curves) and modeled (solid curves) fields for 1991–2000, showing DMI (top panel), SSTA in the western antinode region (middle panel), and SSTA in the eastern antinode region (bottom panel). Both the 1994 and 1997 events and their intraseasonal variabilities are reproduced reasonably well by MR (Fig. 3a), with a model–data DMI correlation of 0.83 above 99.5% red noise significance. During the entire record, interannual variabilities in both the western and eastern tropical Indian Ocean regions are simulated reasonably well (Figs. 3b and 3c), the model–data correlation being 0.74 for the western antinode and 0.81 for the eastern antinode, both values exceeding the 99.5% significance level. In addition to SST, sea level variations at intraseasonal and interannual time scales are well reproduced in solution MR (Fig. 4), the model–data correlation being 0.84 (0.85) for the western (eastern) antinode, exceeding the 99.5% significance level. A further validation of observed and modeled intraseasonal and interannual variabilities is provided in section 3.

Differences between solution MR and the data, however, do exist. The model sometimes significantly underestimates or overestimates the amplitudes of in-

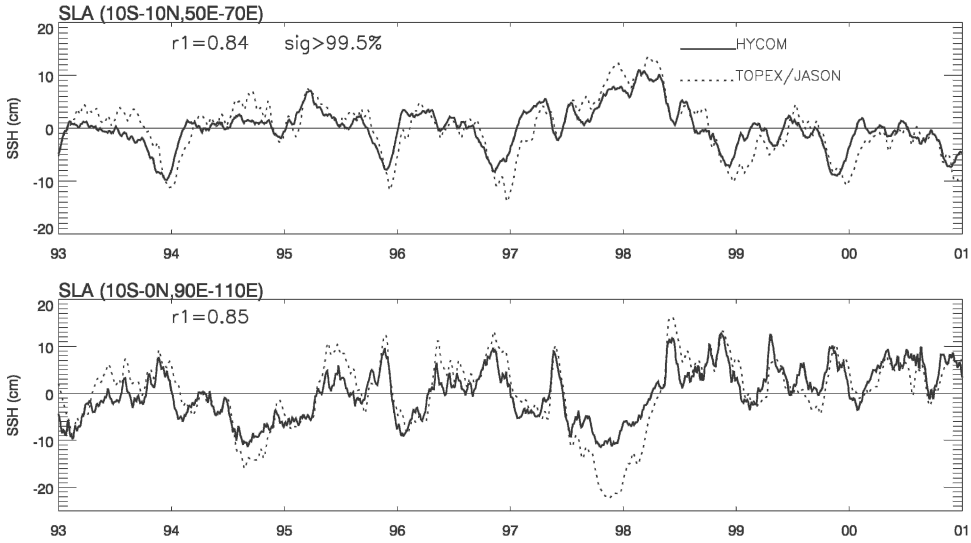

FIG. 4. (a) Time series of SLA from TOPEX/Poseidon altimeter data with a 3-day resolution (dashed curves) in the western antinode region, and from the 3-day-mean MR solution (solid curves) for the period of 1993–2000, a period when the TOPEX/Poseidon data overlap the model integration period. For both curves, their 8-yr 3-day-mean climatologies are removed, and thus values shown in the figure include intraseasonal and interannual variabilities. (b) Same as in (a), but for the eastern antinode region.

traseasonal SST (Fig. 3). Even for the strong 1994 IOZDM, the eastern antinode cooling is overestimated in solution MR (Figs. 1a, 1c, and 3c). For the 1997 IOZDM, the eastern basin cooling extends farther west in MR (Figs. 1b and 1d). These model–data discrepancies may result partly from the uncertainty in the forcing fields, and partly from the inaccuracy of model representations for surface heat fluxes and mixed layer processes. Nevertheless, solution MR produces reasonable intraseasonal-to-interannual SST, sea level, and IOZDM events, which indicates that it captures the major processes that determine the SST and sea level variability in the region, and so is suitable for the purposes of the present study.

3. Results

In this section, we examine the influence of ISOs on the three IOZDM events during the 1990s, beginning with the extremely strong and prolonged 1997 event. For each event, we first provide observational evidence for their impact, and then discuss our numerical solutions to identify the basic processes involved.

a. The 1997 event

1) DATA ANALYSIS

Figures 5a–d plot the observed variables along the equator averaged from 5°S to 5°N for January 1997–February 1998, showing precipitation and winds (Fig. 5a), sea level from TOPEX/Poseidon altimeter data (Fig. 5b), and interannual SSTA from NOAA OI weekly SST data (Fig. 5c), each field bandpassed between 10 and 105 days, as well as interannual SSTA from OI without bandpass filtering (Fig. 5d). Figure 5e is the same as Fig. 5d except for the area 10°S–2°N average, a latitudinal band in which the eastern antinode SSTA is strong (right panels in Fig. 1).

As shown in Figs. 5a and 5b, intraseasonal convection (gray shades in Fig. 5a) and wind frequently occur at 20–60-day periods, whereas the sea level response shifts to longer periods near 90 days (Fig. 5b). For example, strong precipitation occurs in mid-February, the end of March, and early May, whereas SLA maxima appear at the end of February and the end of May in the eastern basin. Wavelet analysis of wind and sea level demonstrates that during spring 1997, equatorial zonal wind has significant power at 30–90-day periods, and SLA is dominated by the near-90-day oscillations (Fig. 6). Indeed, a spectral analysis of an 8-yr (1993–2000) record of TOPEX/Poseidon data shows that intraseasonal sea level is dominated by near-90-day oscillations in the equatorial Indian Ocean, albeit with prominent interannual variations (Han et al. 2001; Han 2005; Fig. 6b). The dominant 90-day SLA results from the winds, which have significant power near 90 days (Han 2005; Fig. 6a), excite a basinwide resonance (section 1; Han 2005). A noteworthy consequence of resonance is

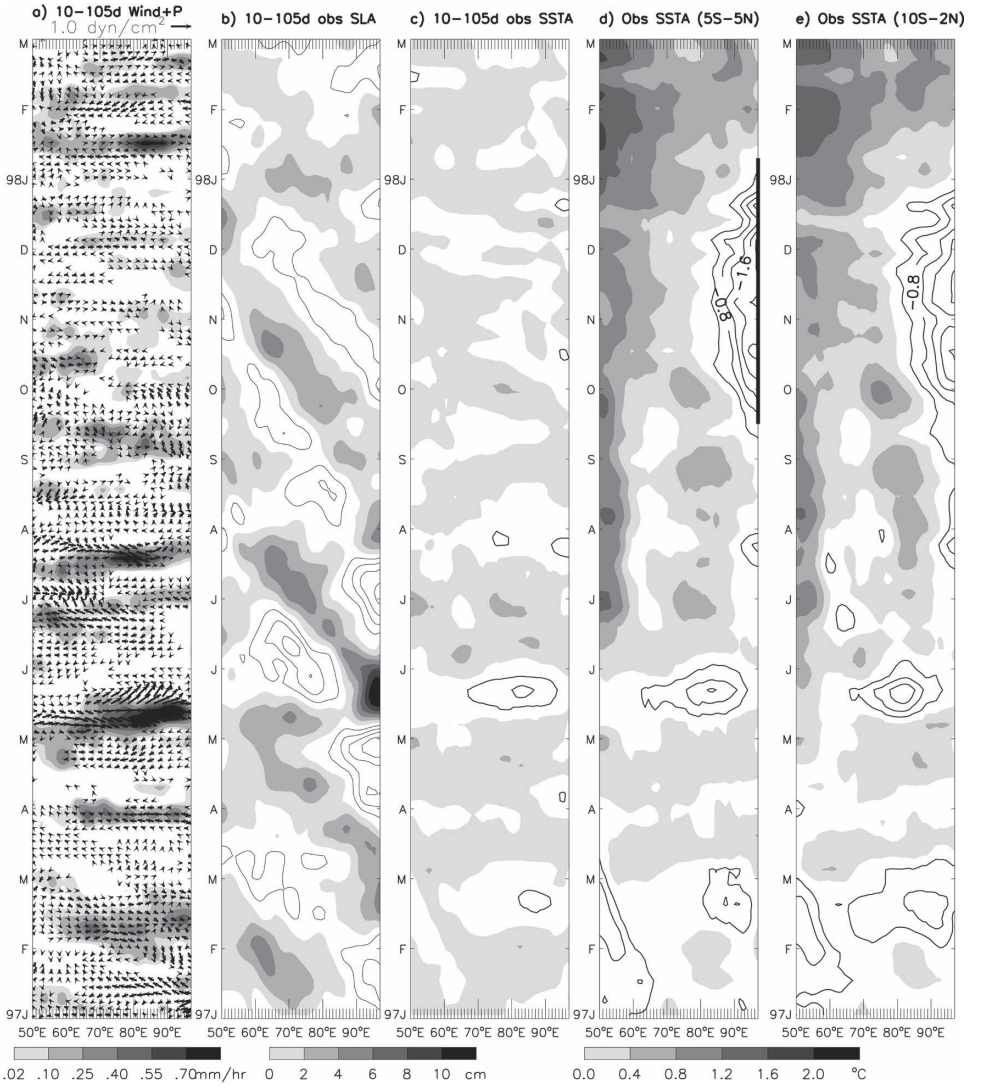

FIG. 5. (a) Longitude–time plot of intraseasonal (10–105 day) ERA-40 wind stress (arrows) and intraseasonal CMAP precipitation (gray shades) averaged over 5°S–5°N of the Indian Ocean during January 1997–February 1998. The Lanczos bandpass filter is applied with half-power points at 10 and 105 days. (b) Same as in (a), but for 10–105-day TOPEX/Poseidon sea level. Positive values are shaded and negative ones are contoured, with an interval of 2 cm. (c) Bandpass-filtered (10–105 day) interannual SSTA from (d). (d) NOAA OI weekly interannual SSTA data averaged over 5°S–5°N, based on the 10-yr (1991–2000) SST data. The weekly climatology for the 10-yr period is removed. The portion of the thick axis on the right-hand side is the time period when the equatorial zonal SST gradient reversed. (e) Same as in (d), but for averaging over 10°S–2°N. Positive values are shaded and negative ones are contoured, with an interval of 0.4°C.

that the 90-day response is not obviously related to the local wind forcing (cf. Figs. 5a and 5b). The resonant response does not require the winds to have a 90-day spectral peak, but it does require the winds to have a significant power at the 90-day period (Han 2005).

Associated with the 90-day resonance is a high sea level signal in the eastern basin during August and early September, coincident with positive SSTA there that delays the reversal of the equatorial, zonal SST gradient in the eastern basin by more than a month (Figs. 5b, 5c, 5d, and 2h). This positive SSTA significantly reduces the negative SSTA in the eastern antinode region and restores the negative SSTA to normal by the end of August (Fig. 5e). Given that the reversal of the equatorial zonal SST gradient marks the beginning of the

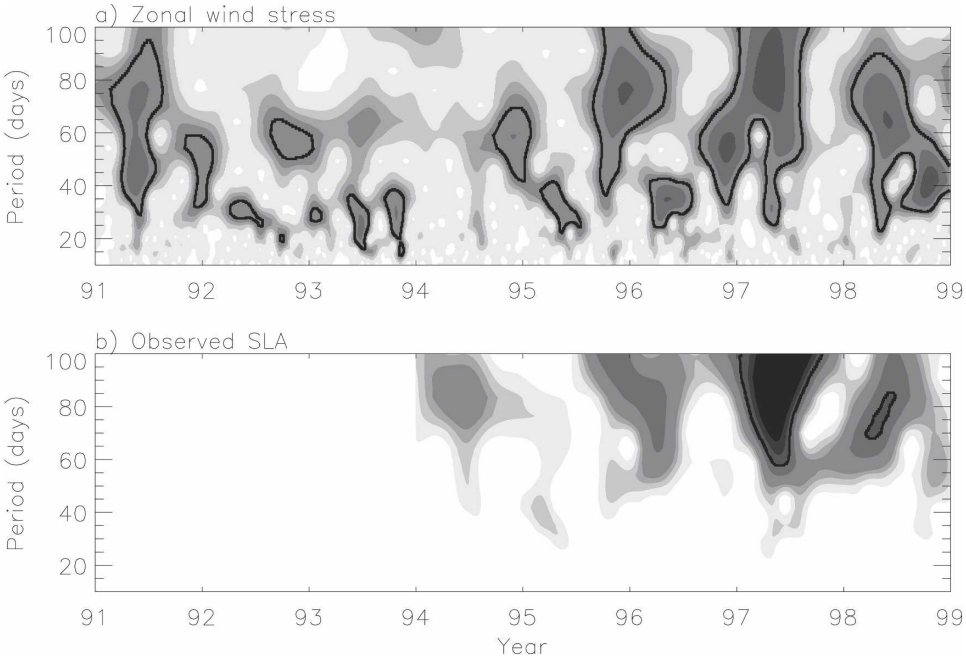

FIG. 6. (a) The local, normalized wavelet power spectra (Torrence and Compo 1998) of ERA-40 zonal wind stress averaged over the central equatorial basin (5°S–5°N, 60°–90°E) for the period of 1991–98. (b) Same as in (a), but for TOPEX/Poseidon SLA averaged in the eastern equatorial basin (5°S–5°N, 80°–100°E) for the period of 1994–98. Darker shading indicates higher power. The contour-enclosed regions are the significance of results exceeding the 95% confidence level.

strong phase of IOZDMs (section 1; Fig. 2), the 90-day resonance delays the starting time for the IOZDM to enter its *strong* phase, although a regular dipole event of 1997 was suggested to begin at an earlier time based on the occurrence of SSTA in the eastern and western antinode regions (e.g., Saji et al. 1999; Webster et al. 1999).

Forcing by ISOs can affect SST by changing the surface fluxes and by wind-driven dynamical adjustments. The close relationship between sea level and SST anomalies indicates that dynamical adjustments are the likely cause for the warm SSTAs that delay the reversal of the equatorial zonal SST gradient and thus delay the strong IOZDM onset [see section 3a(2)].

During the development and termination of the event, atmospheric ISOs do not appear to play a significant role, as they remain weak from mid-September through December in most regions of the equatorial basin, except for the western basin where they are stronger than they are during normal years (Fig. 5a; Shinoda and Han 2005). There is, however, a clear example of their influence during May before the dipole onset. At that time, intraseasonal sea level is high in the eastern equatorial ocean, but SSTAs are negative across the basin with a maximum amplitude exceeding 1°C. This strong surface cooling must therefore be caused by the strong winds and convection associated with the ISO during May, which increases evaporation and entrainment and reduces shortwave radiation. The cooling may also result from anomalous advection due to intraseasonal wind stress forcing.

2) MODEL SOLUTIONS

To isolate the processes by which the ISOs affect SST, we plot difference fields between pairs of solutions to the ocean model. Figure 7 plots fields from the difference between solutions MR and BR (solution MR–BR), which estimates the impact of all intraseasonal forcings (Table 1). It shows longitude–time sections along the equator for the depth of 20°C isotherm (D20; Fig. 7a), SLA (Fig. 7b), and interannual SSTA (Fig. 7c), each bandpassed between 10 and 105 days; also shown is the interannual SSTA from solution MR (Fig. 7d). Note that the thermocline depth mirrors SLA; it shoals (deepens) when sea level drops (rises), demonstrating that most of the sea level variability is baroclinic in nature.

The latter three panels in Fig. 7 generally agree with their counterparts in Fig. 5. For example, the model is able to simulate the ISO-induced interannual cooling during May (Figs. 5c and 7c), the cooling in the central

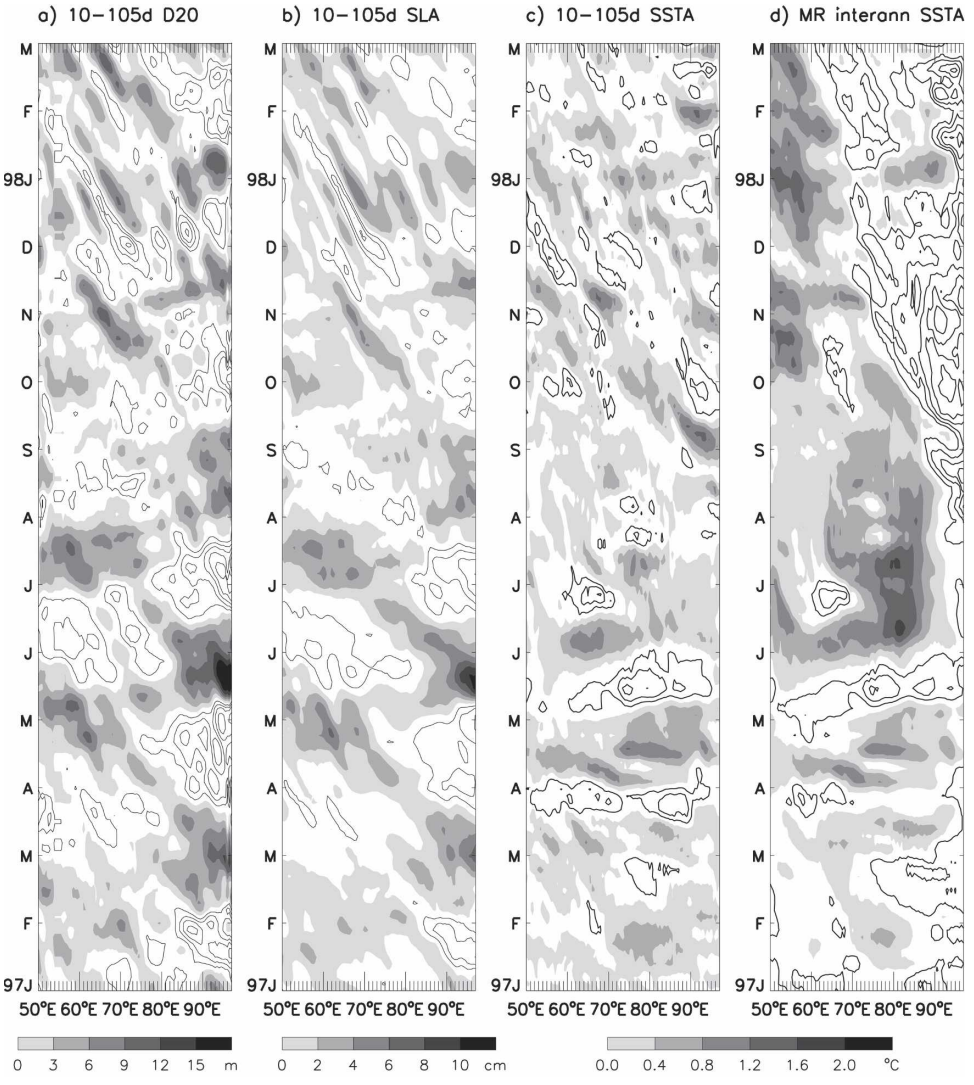

FIG. 7. (a) Longitude–time plot of bandpass-filtered (10–105 day) 20°C isotherm depth (D20) from solution MR–BR averaged over 5°S–5°N of the Indian Ocean during January 1997–February 1998. (b) Same as in (a), but for sea level. (c) Same as in (a), but for interannual SSTA, which is the SSTA from solution MR–BR with its 3-day-mean climatology for 1991–2000 removed. (d) Interannual SSTA from solution MR averaged over 5°S–5°N. The 3-day-mean climatology for 1991–2000 is removed. To eliminate high-frequency noise from solution MR, a low-pass filter is applied with half-power point at 10-day period. Positive values are shaded and negative ones are contoured, with an interval of 2 cm for sea level, 3 m for D20, and 0.4°C for SSTA.

and eastern basins during July, and the warming in the eastern basin during August–September. This warming coincides with the positive SLA associated with the 90-day oscillations and explains the delay of the equatorial zonal SST–gradient reversal (Figs. 5b–d and 7b–d). The negative SSTAs in the east and positive SSTAs in the west associated with the IOZDM during September 1997–January 1998 are also reasonably simulated (Figs. 5d and 7d). The eastern basin cooling, however, extends farther west in the model and is overestimated during August (Figs. 5d and 7d; also see section 2c). Additionally, the observed SLA and SSTA fields are smoother than the modeled ones because mesoscale variability is removed from the TOPEX/Poseidon SLAs (Fu 2004) and the NOAA OI SST has a 1° spatial and weekly temporal resolutions, coarser than 0.5° and 3-day resolutions for HYCOM. Nevertheless, the overall agreement confirms the model's ability to represent the basic processes that determine intraseasonal and interannual variabilities.

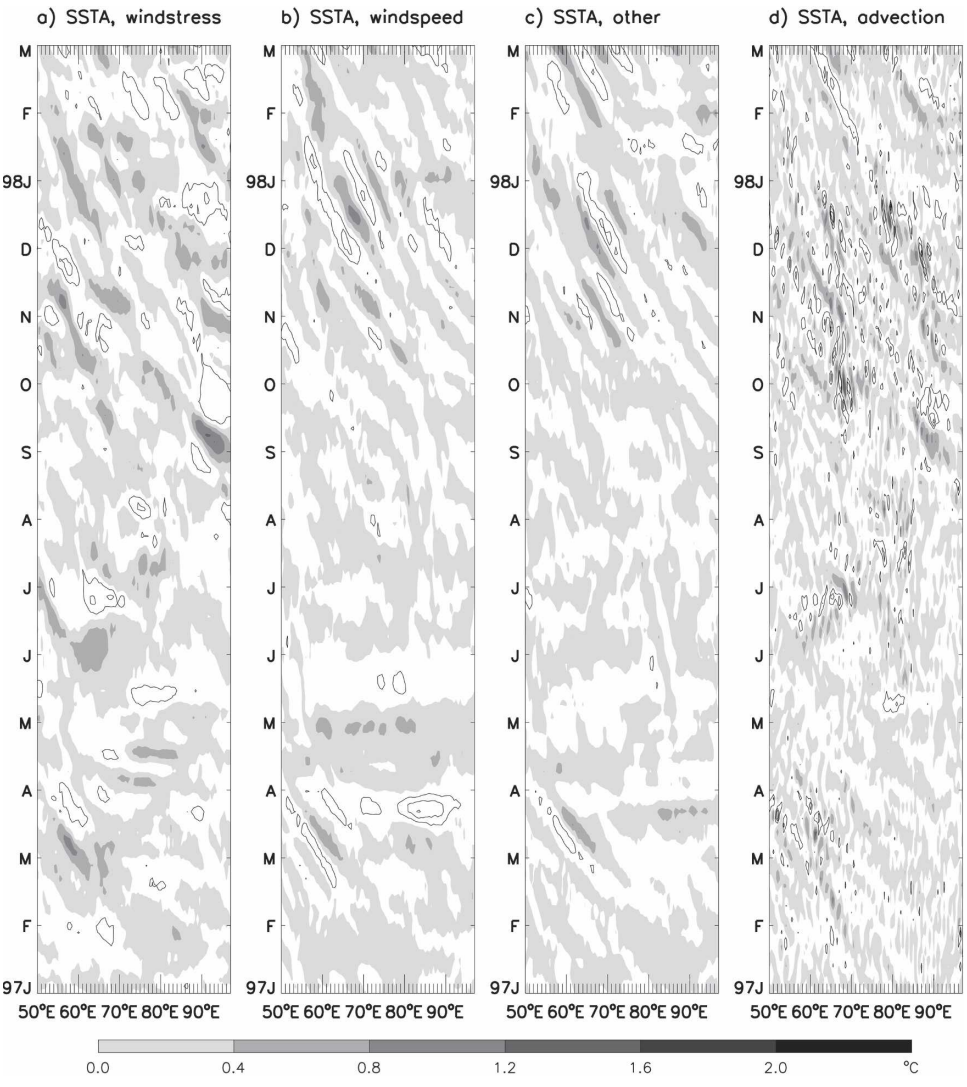

FIG. 8. (a) Longitude–time plot of intraseasonal (10–105 day) SSTA from solution MR–TR1, which isolates the effects of wind stress, averaged over 5°S–5°N of the Indian Ocean during January 1997–February 1998. (b) Same as in (a), but for solution TR1–TR2, which isolates wind speed effects. (c) Same as in (a), but for SSTA from solution TR2–BR, which estimates the effects of intraseasonal forcing other than winds. It primarily represents the effects of intraseasonal radiative fluxes. (d) Same as in (a), but for estimated SSTA caused by ISOs via horizontal advection. See text for detailed description. Positive values are shaded and negative ones are contoured, with an interval of 0.4°C.

Figures 8a–c show SSTAs along the equator from three difference solutions that estimate the influences of forcing by intraseasonal wind stress alone (solution MR–TR1), by wind speed alone (solution TR1–TR2), and by other forcing fields, namely, shortwave and longwave radiation, air temperature, specific humidity, and precipitation (solution TR2–BR). To estimate the impact of ISO-induced advection, Fig. 8d shows

$$\Delta T = -\left[u\frac{\partial T}{\partial x} + v\frac{\partial T}{\partial y} - \left(\overline{u}\frac{\partial \overline{T}}{\partial x} + \overline{v}\frac{\partial \overline{T}}{\partial y} \right) \right] \Delta t, \quad (2)$$

where u, v, and T are the zonal and meridional currents and SST, respectively, from solution MR, and $\overline{u}$, $\overline{v}$, and $\overline{T}$ are the same variables from solution BR. According to (2), ΔT measures the rate of change in SST due to ISO-induced advection for a time interval Δt. The choice of Δt is arbitrary and we choose $\Delta t = 3$ days, the resolution of the forcing for solution MR.

The difference solutions in Fig. 7 corroborate the effect of the 90-day waves in delaying the IOZDM to enter its strong phase, as suggested by the observations in Fig. 5. During June and July, intraseasonal easterly

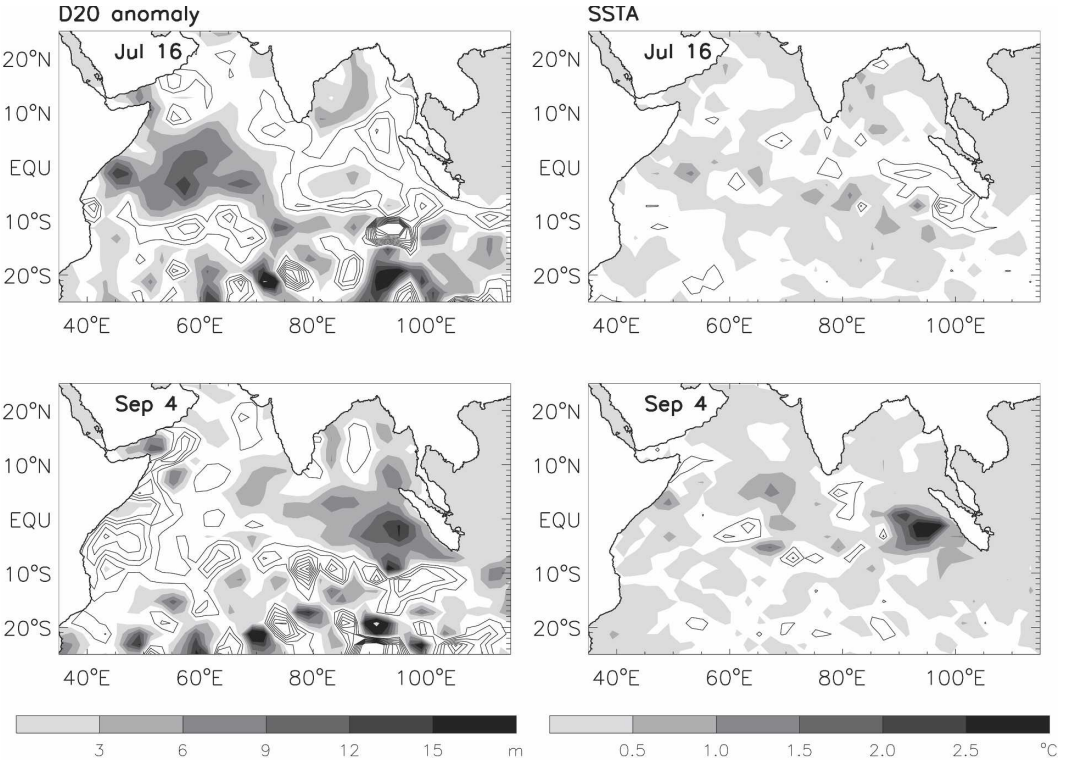

FIG. 9. Variations of (left) D20 and (right) SSTA from solution MR–BR, which isolates the effects of intraseasonal forcing during July and September when atmospheric ISOs impact the onset of the IOZDM. Positive values are shaded and negative ones are contoured, with an interval of 3 m for D20 and 0.5°C for SSTA.

winds (Fig. 5a) act to raise the thermocline in the eastern equatorial ocean (Fig. 7a), enhancing the upwelling associated with the IOZDM there. As a result, SST decreases and the resulting negative SSTAs persist until the end of July (Figs. 7c,d and 5c,d). From late July to mid-September, however, the model thermocline deepens by more than 10 m in the eastern basin because of the 90-day wave (Fig. 7a), reducing or eliminating seasonal upwelling and increasing SST by 0.5°–1.3°C (Figs. 7c,d; 5c,d; and 2h). A comparison of the panels in Fig. 8 confirms these conclusions, showing that the September warming results from forcing by intraseasonal wind stress (Fig. 8a) rather than by intraseasonal surface fluxes (Figs. 8b and 8c). Advection due to ISOs contributes to the westward extension of positive (negative) SSTAs in the eastern basin during early (late) September (Fig. 8d).

Note that the SSTAs in the eastern basin during mid-July to mid-September tend to lag the SLAs (and anomalous thermocline depth) in the same region (Figs. 5b, 5c, and 7a–7c). This is because upwelling affects the time derivative of SST more than it does the SST itself and, hence, the delay. Suppose that an upwelling-favorable Kelvin wave raises the deep thermocline, which is deep enough to inhibit the upwelling of cold subsurface water. At first, there is no effect on SST: Only when the thermocline becomes sufficiently shallow will cool subsurface water finally be able to upwell to the surface. Thereafter, upwelling will continue to cool SST until the thermocline deepens again. Note also that Figs. 5c and 7c show the interannual SSTA with its 3-day mean climatology removed. When sea level first shoals in late June (Figs. 5b and 7b), upwelling associated with the shoaling thermocline will first act to weaken the positive SSTA that occurred earlier (Figs. 5c and 7c); as upwelling continues until the second half of July and thus increases the amount of colder water to the surface, the SSTA becomes progressively cooler and attains its maximum amplitude near the end of July. Effects of local intraseasonal winds complicate the pattern somewhat; but our results above suggest that upwelling is the dominate process for this intraseasonal cooling. Following a similar argument, the warm SSTA at the end of August and early September lags the positive SLA maximum.

The influence of the 90-day wave on the September warming is more apparent in Fig. 9, which shows the spatial structure of D20 (left panels) and SSTA (right

panels) from solution MR–BR during July and early September. During July, the 90-day wave causes the thermocline to shoal in the eastern equatorial ocean and to deepen in the western and central basins near and off the equator (Fig. 9a), a typical first-meridional-mode Rossby wave structure. Associated with this thermocline pattern, SSTA is negative in the eastern equatorial ocean, and positive in the central basin with double maxima off the equator. In contrast, during August to early September the thermocline deepens in the central and eastern equatorial ocean, a typical Kelvin wave structure. The deepened thermocline suppresses equatorial upwelling and increases SST by more than 1.4°C.

As noted above, after the reversal of the zonal SST gradient there are no prominent ISOs during the rest of the IOZDM. There are, however, still intraseasonal SSTAs during dipole development, which cause intraseasonal variations on interannual SSTA (Figs. 7c, d). These SSTAs do not always coincide with thermocline displacements (Figs. 7a and 7c), suggesting the importance of surface heat fluxes and advection (Fig. 8). The SSTAs are generally positive in the western antinode region during January 1998 (Fig. 7c), which may contribute to prolonging the event. This contribution, however, is weak relative to the large-amplitude, interannual SSTAs there (Figs. 5d and 7d).

During May, atmospheric ISOs cause a deepened thermocline in the eastern ocean but a basin-scale cooling, consistent with the observations (cf. Figs. 5c,d and 7c,d). This cooling results mostly from intraseasonal winds (Figs. 8a and 8b), and reduced solar radiation also makes a small contribution (Fig. 8c). Wind speed associated with the ISOs causes strong evaporation and entrainment, resulting in strong cooling (Fig. 8b). Additionally, SSTAs caused only by intraseasonal wind stress are also negative in the central-eastern basin where the thermocline deepens (Fig. 8a). This is because intraseasonal wind stress drives strong intraseasonal currents that advect colder SSTAs south of the equator (not shown) to the central-eastern basin (Fig. 8d). Similar basinwide cooling by an ISO occurs at the end of March, an event that appears to be significantly overestimated by the model. The equatorial westerly wind during May was suggested to affect the circulation in the Indonesian Seas, by exciting equatorial Kelvin waves and subsequent coastal Kelvin waves (Sprintall et al. 2000).

Because of the nonlinearity of the oceanic system, ISO-induced SSTAs can rectify onto the seasonal cycle and interannual variability (Waliser et al. 2003; Han et al. 2004), and thus may exert some influence on the IOZDM. To illustrate rectification, Figs. 10a–c plot SSTAs along the equator low-passed at 105 days from three difference solutions, illustrating the influences of all intraseasonal forcings (solution MR–BR), wind stress alone (solution MR–TR1), and wind speed alone (solution TR1–TR2). The most significant SSTAs are cooling along the equator during April–June and in the eastern basin during July, warming (cooling) in the central-eastern (western) basin during August–October, and warming–cooling in the western basin during December 1997–January 1998. These SSTAs result largely from intraseasonal winds, and wind stress and wind speed have comparable effects (Figs. 10b and 10c). Intraseasonal wind stress can drive large-amplitude thermocline variability that rectifies into low-frequency (lower than intraseasonal time scale) SST variations by the nonlinear, entrainment cooling process. Intraseasonal wind stress can also drive strong intraseasonal currents, which can advect intraseasonal SSTA and thus cause a low-frequency rectification (not shown). Intraseasonal wind speed can cause a rectified SSTA (Fig. 10c) by affecting entrainment cooling.

b. The 1994 event

1) DATA ANALYSIS

For the 1994 dipole, the zonal SST gradient reverses in August (Fig. 2g), although the negative, persistent SSTA in the eastern antinode region occurs earlier (Fig. 11e). The IOZDM reaches a peak during October when the negative SSTA in the eastern antinode and the positive SSTA in the western antinode attain their maxima (Figs. 11d, 11e, and 2g). It then quickly terminates in November.

The strongest intraseasonal event during 1994 is an eastward-propagating disturbance during November (Fig. 11a). As noted by Rao and Yamagata (2004), the rapid and early termination of the event roughly coincides with the November ISO. Note, however, that the ocean warms in the eastern antinode region during late October and early November prior to the ISO event, suggesting that the ISO does not cause the IOZDM termination by warming the eastern antinode region. At the same time, intraseasonal sea level *dropped* by 3–6 cm in the eastern ocean, indicating that ISO-induced thermocline variability is also not the cause. In contrast, in the western antinode region, October warming associated with the ISOs appears to enhance the IOZDM strength and November cooling acts to terminate the positive SSTA of the IOZDM (Figs. 11e and 11d). Earlier in the year, there are moderate intraseasonal perturbations in convection and sea level

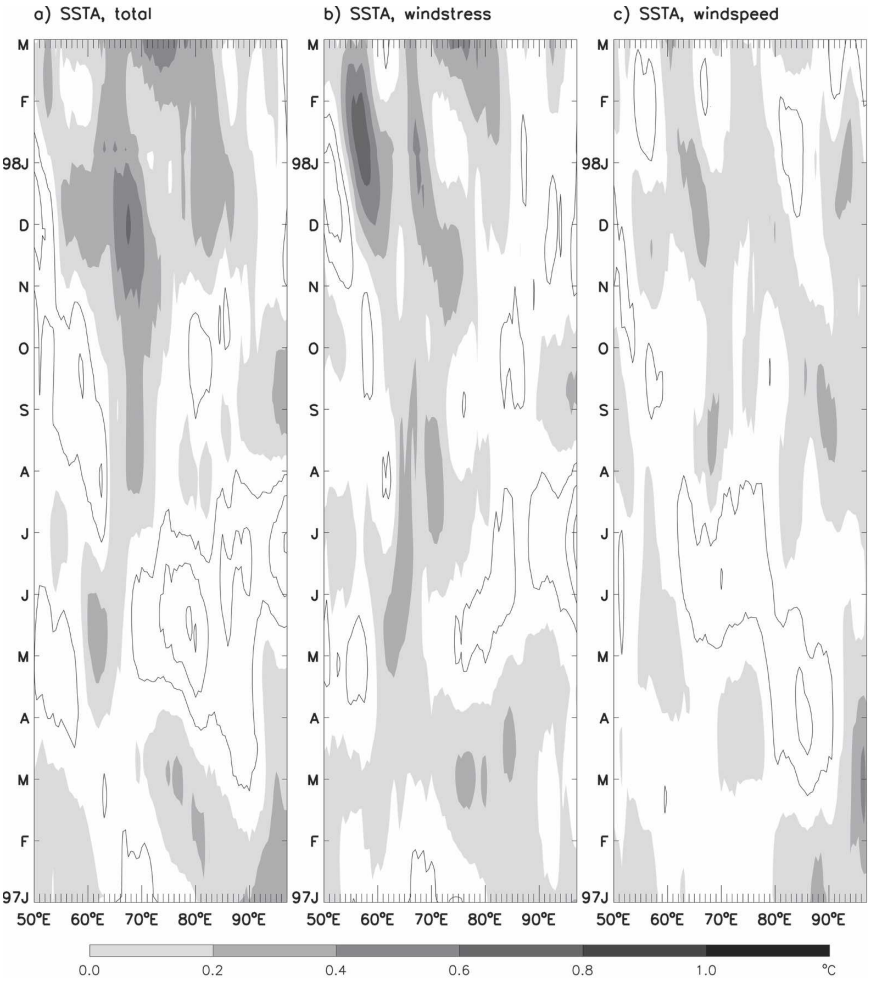

FIG. 10. (a) Longitude–time plot of rectified SSTA forced by ISOs along the Indian Ocean equator (5°S–5°N average during January 1997–February 1998. It is obtained by applying a low-pass 105-day filter to the SSTA from the difference solution (MR–BR). (b) Same as in (a), but for wind stress effects (solution MR–TR1). (c) Same as in (a), but for wind speed effects (solution TR1–TR2). Positive values are shaded and negative ones are contoured, with an interval of 0.2°C. Note that the scale is only one-half of the scale for the SSTA in other figures.

across the equatorial basin, but no obvious SSTAs correspond to them (Fig. 11).

2) MODEL SOLUTIONS

Figures 12 and 13, analogous to Figs. 7 and 8, illustrate the model's response during 1994. Intraseasonal sea level and SSTA variability from the model agree reasonably well with the observations, although there are some differences in amplitudes (Figs. 11b–d and 12b–d). For example, intraseasonal cooling during September, warming during October, and cooling again during November are all well simulated by the model (Figs. 11c and 12c). Sea level is high (low) in the western-central (eastern) basin during November, and is high in the eastern ocean during December.

Consistent with the data analysis, the strongest ISO influence on the IOZDM is the cooling during November and warming during October in the western antinode region. Anomalous convection and westerly winds associated with the November ISO begin in the western basin during early November, and they propagate to the eastern ocean from November to December (Figs. 11a, 2c, and 2g). The ISO cools the SST in the western and central basins (Fig. 11c), thereby terminating the positive SSTA of the IOZDM and thus contributing to the termination of the event. The cooling results primarily from intraseasonal wind stress and wind speed (Figs. 13a and 13b) with a smaller contribution from the reduced shortwave radiation caused by convection (Fig. 13c).

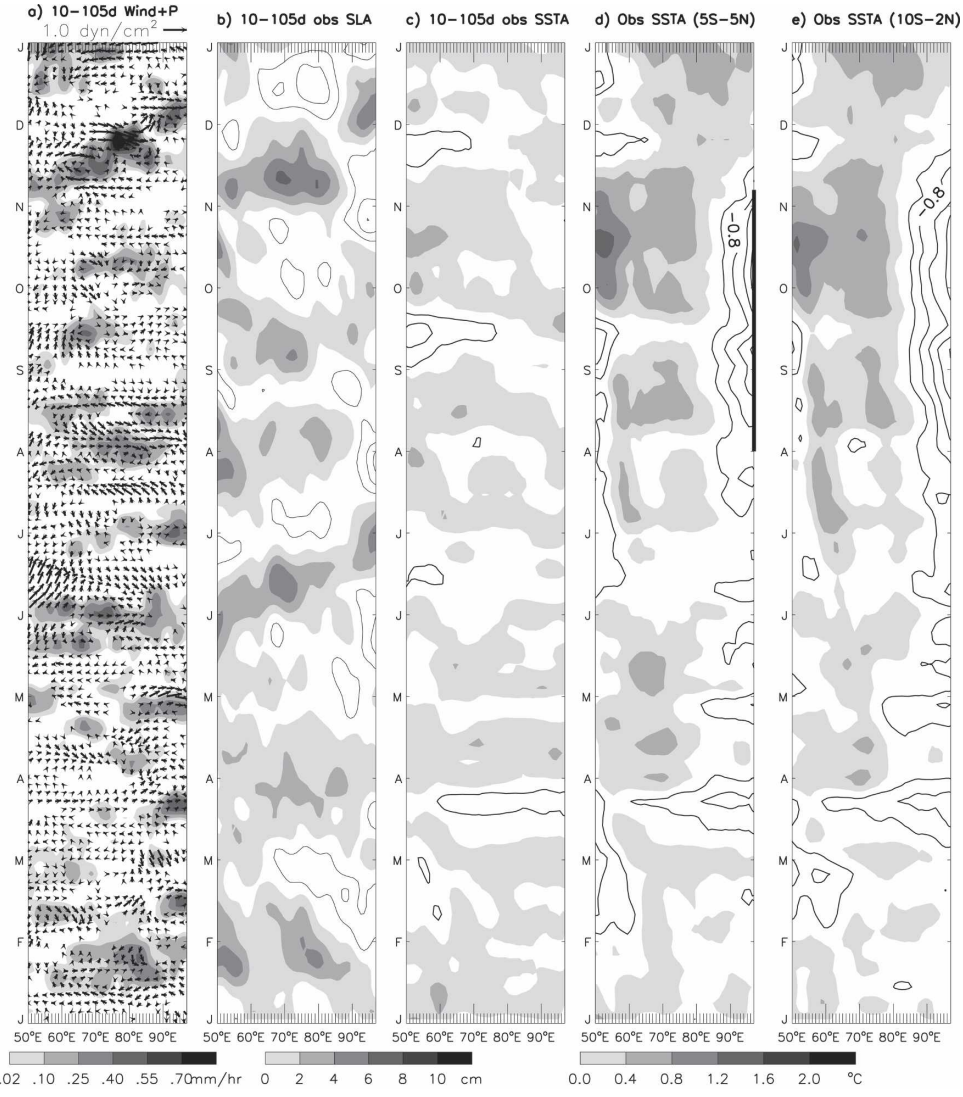

FIG. 11. (a) Longitude–time plot of bandpass-filtered (10–105 day) ERA-40 wind stress (arrows) and intraseasonal CMAP precipitation (gray shades) averaged over 5°S–5°N of the Indian Ocean during 1994. (b) Same as in (a), but for 10–105-day TOPEX/Poseidon SLA. Positive values are shaded and negative ones are contoured, with an interval of 2 cm. (c) Bandpass-filtered (10–105 day) interannual SSTA from (d). (d) NOAA OI weekly interannual SSTA data averaged over 5°S–5°N, based on the 10-yr (1991–2000) SST data. The weekly climatology for the 10-yr period is removed. The portion of the thick axis on the right-hand side is the time period when the equatorial zonal SST gradient reversed. (e) Same as in (d), but for averaging over 10°S–2°N. Positive values are shaded and negative ones are contoured, with an interval of 0.4°C.

In the east, the negative SSTA returns to normal in mid-November (Fig. 11d), and the zonal SST gradient reverses to become eastward (Fig. 2g). As the maximum SST shifts eastward from October to November, convection also moves eastward. Consequently, the eastward *propagation* of the ISO event might be the outcome of the western basin cooling and eastern basin warming, rather than the cause of the warming because the warm SST leads the strongest convection. This result appears to be different from Rao and Yamagata (2004), who suggested that reduced upwelling caused by the ISO is the cause of the eastern basin warming.

In the beginning of November, ISOs do cause a positive SSTA in the eastern ocean in a narrow band in both the data and model, first at the coast and then somewhat offshore (Figs. 11c and 12c). Figure 13a indicates that the primary cause is ISO-related wind stress anomalies, which cause the same narrow SSTA

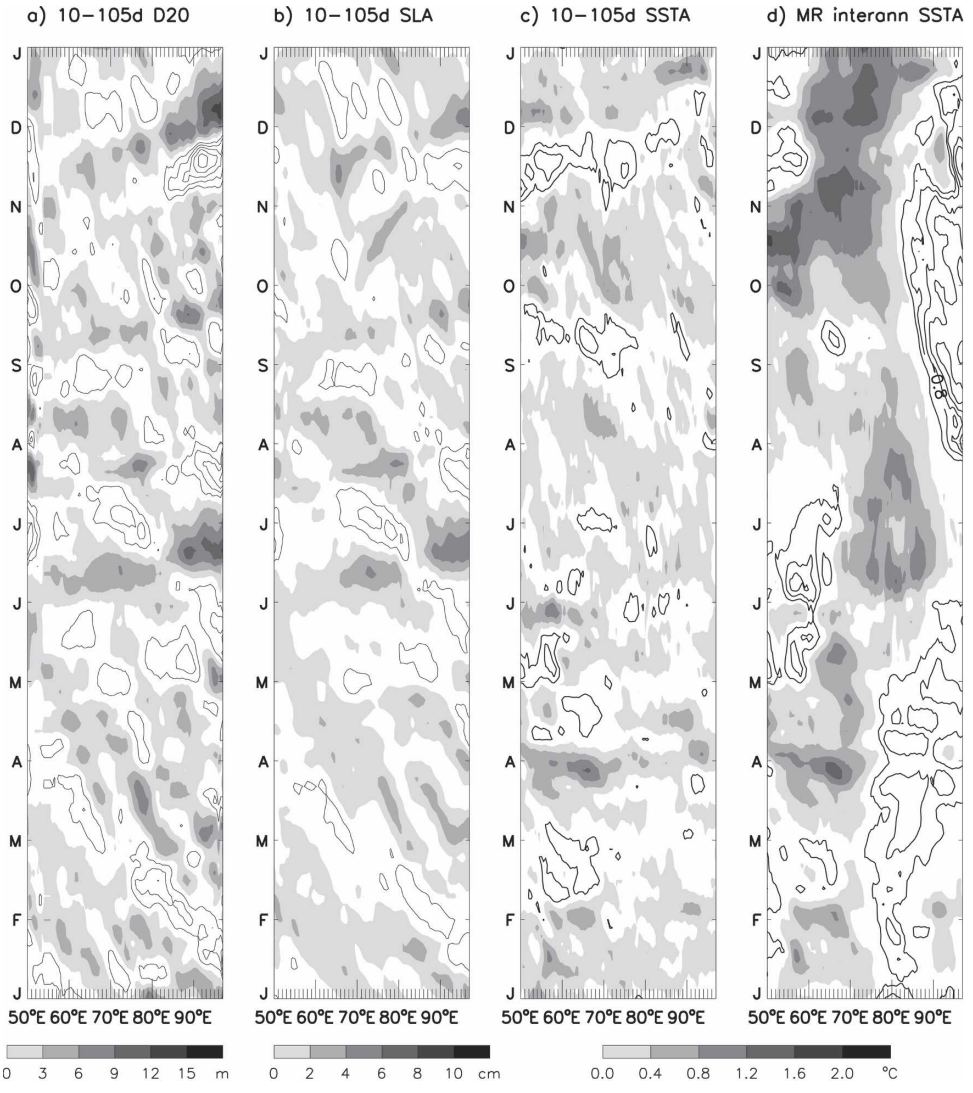

Fig. 12. (a) Longitude–time plot of bandpass-filtered (10–105 day) 20°C isotherm depth (D20) from solution MR–BR averaged over 5°S–5°N of the Indian Ocean during 1994. (b) Same as in (a), but for sea level. (c) Same as in (a), but for interannual SSTA, which is the SSTA from solution MR–BR with its 3-day-mean climatology for 1991–2000 removed. (d) Interannual SSTA from solution MR averaged over 5°S–5°N. The 3-day-mean climatology for 1991–2000 is removed. To eliminate high-frequency noise from solution MR, a low-pass filter is applied with its half-power point at 10-day period. Positive values are shaded and negative ones are contoured, with an interval of 2 cm for sea level, 3 m for D20, and 0.4°C for SSTA.

pattern as shown in Figs. 12c and 12d, and this SSTA pattern results largely from the advection effect (Fig. 13d). In fact, wind anomalies south of the equator force the warming, and the northwestward-flowing seasonal currents associated with the IOZDM subsequently advect the warmer water equatorward and offshore (not shown). This advective warming, however, is too weak to terminate the eastern antinode cooling. The SST in the eastern basin warms by 1.2°–1.6°C from mid-October to mid-November (Figs. 11d and 12d), whereas the positive intraseasonal SSTA in early November is less than 0.4°C in the data and 0.8°C in the model (Figs. 11c and 12c). What then is the major reason for the eastern antinode warming? Recent work by Halkides (2005) suggests that the seasonal cycle of winds contributes to the 1994 IOZDM termination. A detailed investigation on the causes that terminate the IOZDM is beyond the scope of this study, which focuses on understanding how ISOs affect IOZDM events.

During July and August, when southeasterly winds

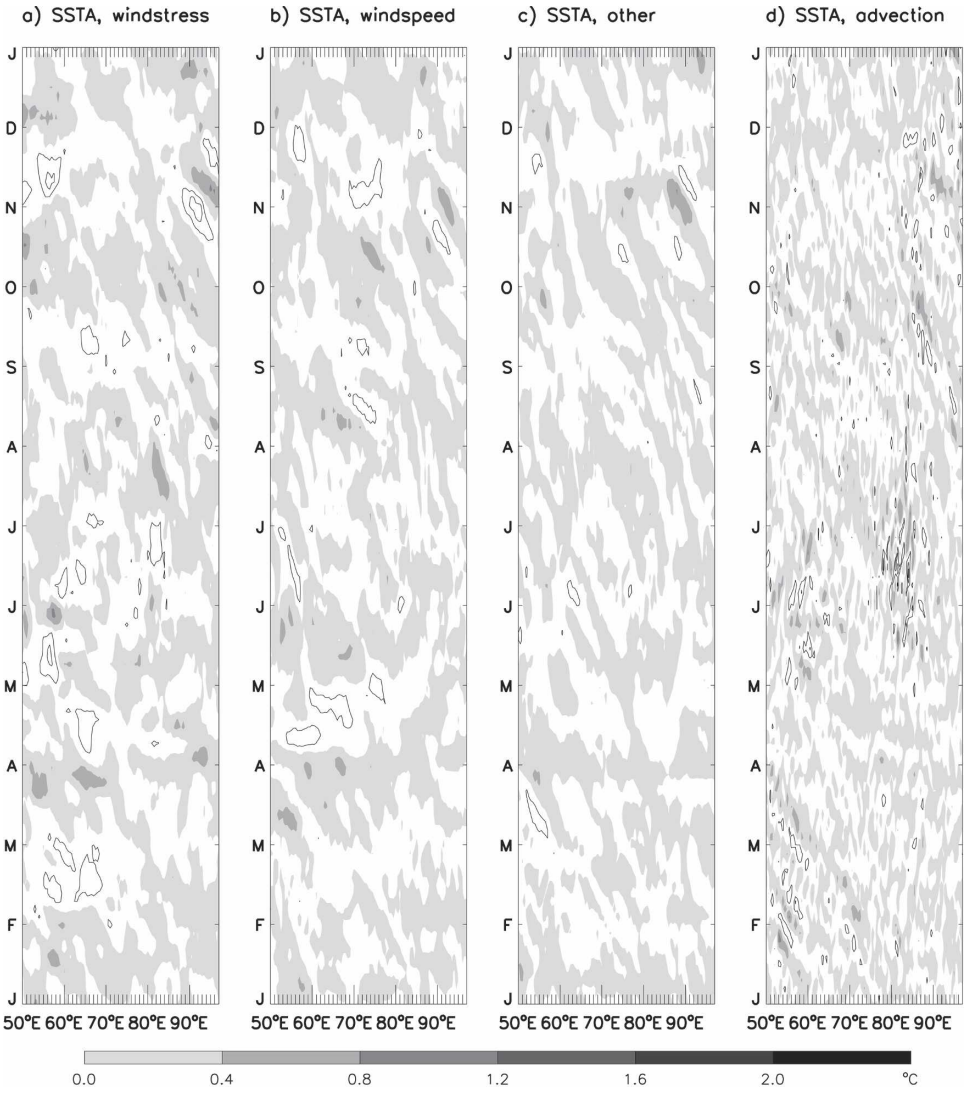

FIG. 13. (a) Longitude–time plot of intraseasonal (10–105 day) SSTA from solution MR–TR1, which isolates the effects of wind stress, averaged over 5°S–5°N of the Indian Ocean during 1994. (b) Same as in (a), but for solution TR1–TR2, which isolates wind speed effects. (c) Same as in (a), but for SSTA from solution TR2–BR, which estimates the effects of intraseasonal forcing other than winds. It primarily represents the effects of intraseasonal radiative fluxes. (d) Same as in (a), but for estimated SSTA caused by ISOs via horizontal advection. See text for detailed description. Positive values are shaded and negative ones are contoured, with an interval of 0.4°C.

cause upwelling in the eastern equatorial basin and the IOZDM begins (Fig. 2c), ISO-induced SSTAs are generally less than 0.4°C across the basin (Fig. 12c), indicating that ISOs do not significantly impact the IOZDM onset, which is consistent with the preceding data analysis. The ISOs, however, do influence the IOZDM peak. During October, when the IOZDM attains a maximum zonal SST gradient (Fig. 2g), ISO-induced interannual SSTAs are positive in the western antinode region with an amplitude of 0.5°–1°C and are weakly negative in the eastern basin (Fig. 12c), intensifying the dipole strength. Indeed, without intraseasonal forcing (solution BR), the period of warmest SSTAs occurs in November, whereas with intraseasonal forcing (solution MR) it occurs in mid-October (not shown), in agreement with the observations. The western warming results primarily from the intraseasonal wind stress forcing a deepened thermocline (Fig. 13a), and advection in the offshore region may have some contribution (Fig. 13d). At the same time, northeasterly winds associated with the ISOs tend to weaken the seasonal southwesterly wind speed in the western equato-

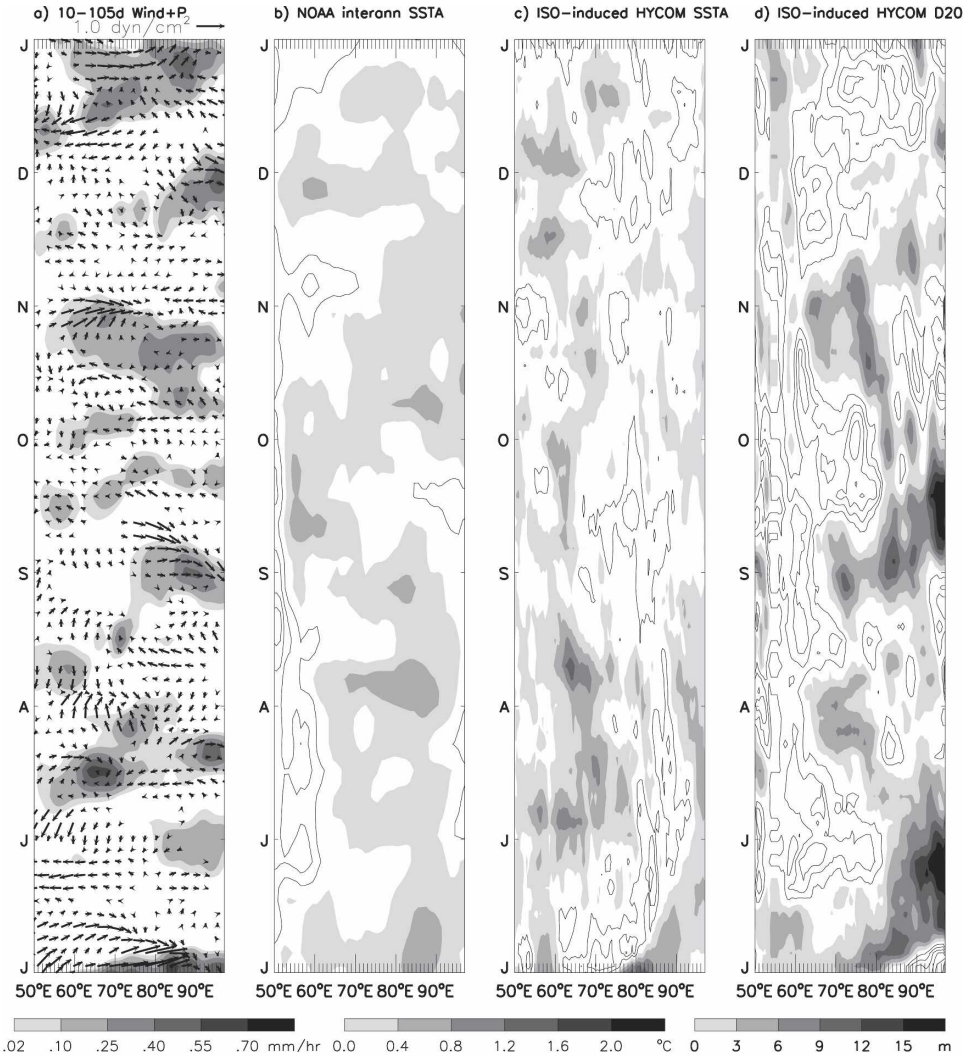

FIG. 14. (a) Longitude–time plot of bandpass-filtered (10–105 day) ERA-40 wind stress (arrows) and intraseasonal CMAP precipitation (gray shades) averaged over 5°S–5°N of the Indian Ocean during June–December of 1991. (b) NOAA OI weekly interannual SSTA data averaged over 5°S–5°N during June–December of 1991, based on the 10-yr (1991–2000) SST data. The weekly climatology for the 10-yr period is removed. (c) SSTA from solution MR–BR, which isolates the effects of ISOs. The 10-yr 3-day-mean climatology is removed. Note that it is not bandpass filtered, and thus the SSTA also includes rectification effects. To remove high-frequency noise, a low-pass filter is applied with its half-power point at 10-day period. (d) Same as in (c), but for D20. Positive values are shaded and negative ones are contoured, with an interval of 0.4°C for SSTA and 3 m for D20.

rial ocean during October (not shown), reducing the total wind speed, decreasing evaporation and entrainment cooling, and thereby increasing SST (Fig. 13b).

c. The 1991 weak event

During 1991, southeasterly winds in the eastern equatorial basin during July–October (Fig. 2b) cause upwelling and thus reduce the warm-pool SST (Figs. 2f and 14b). The zonal SST gradient, however, is not reversed, and intraseasonal convection and their associated westerly winds frequently occur throughout the year (Figs. 2f, 14a, and 6a).

Winds associated with the ISOs generate large-amplitude thermocline variations, with an obvious 90-day oscillation occurring in the eastern basin during June–September (Figs. 6a and 14d). Associated with the 90-day wave, the thermocline is deeper than normal by more than 10 m during June and September. The thermocline shoals during late July and August, but the shoaling is confined to the eastern boundary and is con-

siderably weaker than the deepening. This asymmetry is because higher-frequency ISOs tend to deepen the thermocline at this time, reducing the shoaling by 90-day waves. Corresponding to the deep thermocline, ISO-induced SSTAs are generally positive east of 90°E from June to early October (Fig. 14c). An exception is during early September, when strong winds and convection associated with the ISOs act to cool the SST somewhat in the eastern basin (Figs. 14a and 14c). Note that Figs. 14c and 14d are not bandpass filtered, and therefore they also include the rectification effects of ISOs. The overall effect of the ISOs is to warm the eastern ocean, which reduces cooling by upwelling associated with the weak dipole (cf. Figs. 14c and 14b) and contributes to the premature termination of the weak event. The SSTAs in the eastern equatorial basin become positive by the end of September.

4. Summary and discussion

In this paper, the impacts of atmospheric ISOs on IOZDM events (Fig. 1) are investigated by analyzing available data and performing ocean model experiments. The 3-day-mean ERA-40 winds and CMAP pentad precipitation are analyzed to document atmospheric ISOs during normal, weak-IOZDM, and strong-IOZDM years (Figs. 2a–d, 5a, 11a, and 14a). In addition, 3-day-mean TOPEX/Poseidon sea level and NOAA OI weekly SST data are analyzed to provide evidence for the potential ISO impact on the onset, development, and termination of the dipole events (Figs. 2, 5, 11, and 14). To help understand the processes involved, a suite of ocean model experiments covering the period 1988–2001 are obtained using a version of HYCOM confined to the tropical Indian Ocean. Solution MR is forced by the 3-day-mean ERA-40 fields, CMAP pentad precipitation, and 3-day ISCCP radiative fluxes, whereas solution BR is forced by the low-passed version of the above fields, using a Lanczos digital filter with the half-power point at 105 days. Two additional experiments are performed, allowing estimates of the separate effects of intraseasonal wind stress, wind speed, and other factors (e.g., radiative fluxes) to be assessed.

Our results demonstrate that atmospheric ISOs can have a significant impact on the onset and termination of strong dipole events, causing them to be irregular. Our most prominent result is that a basinwide resonance of Kelvin and Rossby waves near the 90-day period in the equatorial Indian Ocean can cause large-amplitude thermocline variability, delaying the reversal of the equatorial zonal SST gradient (an important indicator for a strong IOZDM) of 1997 by over a month (section 3a). Because of the resonance, sea level and thermocline depth have their strongest response near the 90-day period (Fig. 6), although zonal winds that force the ocean generally have their strongest spectral peaks at 30–60 days (Han 2005). Associated with the resonant 90-day waves, sea level is high and the thermocline is deep in the eastern equatorial Indian Ocean during August and early September (Figs. 5 and 7), which reduce the equatorial upwelling caused by the anomalously strong, seasonal southeasterly winds and, thus, weaken the eastern antinode cooling and delay the reversal of equatorial zonal SST gradient. For the 1997 IOZDM, the zonal SST gradient reverses in mid-September in the warm-pool region (Fig. 2h), in contrast to the 1994 dipole whose SST gradient reverses in early August (Fig. 2g; section 3b). In responding to the reversed SST gradient, ISOs are significantly reduced or even disappear in the central and eastern equatorial Indian Ocean, although they are somewhat enhanced in the western basin (Fig. 2d). Consequently, ISOs do not have a significant effect on the development and termination of the 1997 IOZDM.

The resonant excitation of Kelvin and Rossby waves at the 90-day period does not require zonal winds to have a 90-day peak. It does, however, require the winds to have power at 90 days. A likely source of this power is intraseasonal variability associated with the ISOs, which covers a broad spectral band (G. Kiladis 2004, personal communication). Another possible source is the climatological annual cycle, for which higher harmonics are not negligible.

Interestingly, winds at the 90-day period have an evident interannual variability. During both the 1997 strong IOZDM and 1991 weak IOZDM, zonal winds have significant power at the 90-day period (Fig. 6) and resonant waves are evident. The deepened thermocline associated with a 90-day oscillation during June and September 1991 contributes to the premature termination of the weak dipole (Fig. 14; section 3c). Given that the strong IOZDM events usually last only for 3–4 months (90–120 days), a significant impact of ISOs on the IOZDM through the 90-day waves is expected.

During 1994, winds at the 90-day period are weak and thus 90-day waves are not strongly excited (Fig. 6). Instead, a strong ISO event during November contributes to the early and quick termination of the IOZDM primarily by cooling the western antinode region. This cooling arose from increased evaporation and entrainment, wind stress–induced thermocline variability, and reduced incoming solar radiation due to increased convection (Figs. 11c, 12c, and 13; section 3b). Additionally, the ISOs considerably enhanced the western basin warming during October, intensifying the dipole

strength. In the east, warming due to ISOs in early November resulted primarily from horizontal advection, and this warming contributes only somewhat to the IOZDM termination (section 3b).

These results suggest that for the strong dipole events, southeasterly winds are sufficiently strong in the eastern tropical Indian Ocean for upwelling to reverse the zonal SST gradient along the equator. For these cases, atmospheric ISOs are significantly weakened in the central and eastern equatorial ocean but are enhanced in the western basin (Fig. 2). Consequently, ISOs can have a significant impact on the strong IOZDM onset by affecting its eastern antinode, when the ISOs are not modulated by the IOZDM (such as the 1997 event). Once the strong dipole begins, the ISOs can also affect the IOZDM development and termination primarily through influencing the western antinode region, where ISOs are enhanced by the reversed SST gradient (such as the 1994 event). For the weak dipole, however, the anomalous southeasterlies are not so strong. The deepened thermocline associated with the resonant 90-day waves can further weaken and terminate the event.

Acknowledgments. We thank ECMWF and NCAR for the ERA-40 fields, the NOAA–CIRES Climate Diagnostics Center for the NOAA optimum interpolation SST and CMAP precipitation data, and Dr. Yuanchong Zhang for the ISCCP flux data. All of these datasets are made available through the Internet. Weiqing Han is supported by NSF Grants OCE-0136836 and OCE-0452917, Toshiaki Shinoda by CLIVAR-Pacific grants from NOAA's Office of Global Programs and NSF Grant OCE-0453046, Lee-Lueng Fu by the NASA Jason and TOPEX/Jason projects at the Jet Propulsion Laboratory of the California Institute of Technology, and Julian P. McCreary by the Japan Agency for Marine–Earth Science and Technology (JAMSTEC) through its sponsorship of the International Pacific Research Center (IPRC).

REFERENCES

Annamalai, H., R. Murtugudde, J. Potemra, S. P. Xie, P. Liu, and B. Wang, 2003: Coupled dynamics over the Indian Ocean: Spring initiation of the zonal mode. *Deep-Sea Res.,* **50B,** 2305–2330.

——, J. Potemra, R. Murtugudde, and J. P. McCreary, 2005: Effect of preconditioning on the extreme climate events in the tropical Indian Ocean. *J. Climate,* **18,** 3450–3469.

Bleck, R., 2002: An oceanic general circulation model framed in hybrid isopycnic–Cartesian coordinates. *Ocean Modell.,* **4,** 55–88.

Duchon, C. E., 1979: Lanczos filtering in one and two dimensions. *J. Appl. Meteor.,* **18,** 1016–1022.

Fu, L.-L., 2003: Wind-forced intraseasonal sea level variability of the extratropical oceans. *J. Phys. Oceanogr.,* **33,** 436–449.

——, 2004: Latitudinal and frequency characteristics of the westward propagation of large-scale oceanic variability. *J. Phys. Oceanogr.,* **34,** 1907–1921.

Halkides, D., 2005: The effects of seasonal cycle on the development and termination of the Indian Ocean zonal mode. Ph.D. dissertation, University of Colorado, Boulder, CO, 166 pp.

Halliwell, G. R., 1998: Simulation of North Atlantic decadal/multi-decadal winter SST anomalies driven by basin-scale atmospheric circulation anomalies. *J. Phys. Oceanogr.,* **28,** 5–21.

——, 2004: Evaluation of vertical coordinate and vertical mixing algorithms in the Hybrid Coordinate Ocean Model (HYCOM). *Ocean Modell.,* **7,** 285–322.

Han, W., 2005: Origins and dynamics of the 90-day and 30–60-day variations in the equatorial Indian Ocean. *J. Phys. Oceanogr.,* **35,** 708–728.

——, J. P. McCreary, D. L. T. Anderson, and A. J. Mariano, 1999: Dynamics of the eastward surface jets in the equatorial Indian Ocean. *J. Phys. Oceanogr.,* **29,** 2191–2209.

——, D. M. Lawrence, and P. J. Webster, 2001: Dynamical response of equatorial Indian Ocean to intraseasonal winds: Zonal flow. *Geophys. Res. Lett.,* **28,** 4215–4218.

——, P. J. Webster, R. Lukas, P. Hacker, and A. Hu, 2004: Impact of atmospheric intraseasonal variability in the Indian Ocean: Low-frequency rectification in equatorial surface current and transport. *J. Phys. Oceanogr.,* **34,** 1350–1372.

Hendon, H. H., and M. L. Salby, 1996: Planetary-scale circulations forced by intraseasonal variations of observed convection. *J. Atmos. Sci.,* **53,** 1751–1758.

Jensen, T. G., 1993: Equatorial variability and resonance in a wind-driven Indian Ocean model. *J. Geophys. Res.,* **98,** 22 533–22 552.

Jerlov, N. G., 1976: *Marine Optics.* Elsevier, 231 pp.

Kessler, W. S., and R. Kleeman, 2000: Rectification of the Madden–Julian oscillation into the ENSO cycle. *J. Climate,* **13,** 3560–3575.

Kiladis, G., and K. Straub, 2001: Forcing of the equatorial ocean by an atmospheric Kelvin wave. Preprints, *13th Conf. on Atmospheric and Oceanic Fluid Dynamics,* Breckenridge, CO, Amer. Meteor. Soc., 283–286.

Knutson, T. R., and K. M. Weickmann, 1987: 30–60 day atmospheric oscillations: Composite life cycles of convection and circulation anomalies. *Mon. Wea. Rev.,* **115,** 1407–1436.

Krishnamurti, T. N., and D. Subramanyam, 1982: The 30–50 day mode at 850 mb during MONEX. *J. Atmos. Sci.,* **39,** 2088–2095.

Large, W. G., J. C. McWilliams, and S. C. Doney, 1994: Oceanic vertical mixing: A review and a model with a nonlocal boundary layer parameterization. *Rev. Geophys.,* **32,** 363–403.

——, G. Danabasoglu, S. C. Doney, and J. C. McWilliams, 1997: Sensitivity to surface forcing and boundary layer mixing in a global ocean model: Annual-mean climatology. *J. Phys. Oceanogr.,* **27,** 2418–2447.

Lau, K.-M., and P. H. Chan, 1988: Intraseasonal and interannual variations of tropical convection: A possible link between the 40–50 day oscillation and ENSO. *J. Atmos. Sci.,* **45,** 506–521.

Lawrence, D. M., and P. J. Webster, 2001: Interannual variations of the intraseasonal oscillation in the south Asian summer monsoon region. *J. Climate,* **14,** 2910–2922.

Levitus, S., and T. P. Boyer, 1994: *Temperature.* Vol. 4, *World Ocean Atlas 1994,* NOAA Atlas NESDIS 4, 117 pp.

——, R. Burgett, and T. P. Boyer, 1994: *Salinity.* Vol. 3, *World Ocean Atlas 1994,* NOAA Atlas NESDIS 3, 99 pp.

Madden, R. A., and P. R. Julian, 1971: Detection of a 40–50 day oscillation in the zonal wind of the tropical Pacific. *J. Atmos. Sci.,* **28,** 702–708.

——, and ——, 1972: Description of global-scale circulation cells in the Tropics with a 40–50 day period. *J. Atmos. Sci.,* **29,** 1109–1123.

Masumoto, Y., H. Hase, Y. Kuroda, H. Matsuura, and K. Takeuchi, 2005: Intraseasonal variability in the upper-layer currents observed in the eastern equatorial Indian Ocean. *Geophys. Res. Lett.,* **32,** L02607, doi:10.1029/2004GL021896.

McPhaden, M. J., 1999: Genesis and evolution of the 1997–98 El Niño. *Science,* **283,** 950–954.

Moore, A. M., and R. Kleeman, 1999: Stochastic forcing of ENSO by the intraseasonal oscillation. *J. Climate,* **12,** 1199–1220.

Murtugudde, R., and A. Busalacchi, 1999: Interannual variability of the dynamics and thermodynamics of the tropical Indian Ocean. *J. Climate,* **12,** 2300–2326.

——, B. N. Goswami, and A. Busalacchi, 1998: Air–sea interaction in the Southern Tropical Indian Ocean and its relation to interannual variability of the monsoon over India. *Proc. Int. Conf. on Monsoon and Hydrology,* Kyongju, Korea, CLIVAR/Monsoon Panel, 184–188.

——, J. P. McCreary, and A. J. Busalacchi, 2000: Oceanic processes associated with anomalous events in the Indian Ocean with relevance to 1997–1998. *J. Geophys. Res.,* **105,** 3295–3306.

Rao, S. A., and T. Yamagata, 2004: Abrupt termination of Indian Ocean dipole events in response to intraseasonal oscillations. *Geophys. Res. Lett.,* **31,** L19306, doi:10.1029/2004GL020842.

Reppin, J., F. A. Schott, J. Fischer, and D. Quadfasel, 1999: Equatorial currents and transports in the upper central Indian Ocean: Annual cycle and interannual variability. *J. Geophys. Res.,* **104,** 15 495–15 514.

Reynolds, R. W., N. A. Rayner, T. M. Smith, D. C. Stokes, and W. Wang, 2002: An improved in situ and satellite SST analysis for climate. *J. Climate,* **15,** 1609–1625.

Saji, N. H., B. N. Goswami, P. N. Vinayachandran, and T. Yamagata, 1999: A dipole mode in the tropical Indian Ocean. *Nature,* **401,** 360–363.

Schiller, A., and J. S. Godfrey, 2003: Indian Ocean intraseasonal variability in an ocean general circulation model. *J. Climate,* **16,** 21–39.

Schouten, M. W., W. P. M. de Ruijter, P. J. van Leeuwin, and H. A. Dijkstra, 2002: An oceanic teleconnection between the equatorial and southern Indian Ocean. *Geophys. Res. Lett.,* **29,** 1812, doi:10.1029/2001GL014542.

Senan, R., D. Sengupta, and B. N. Goswami, 2003: Intraseasonal monsoon jets in the equatorial Indian Ocean. *Geophys. Res. Lett.,* **30,** 1750, doi:10.1029/2003GL017583.

Sengupta, D., R. Senan, and B. N. Goswami, 2001: Origin of intraseasonal variability of circulation in the tropical central Indian Ocean. *Geophys. Res. Lett.,* **28,** 1267–1270.

Shinoda, T., and H. H. Hendon, 1998: Mixed layer modeling of intraseasonal variability in the tropical western Pacific and Indian Oceans. *J. Climate,* **11,** 2668–2685.

——, and W. Han, 2005: Influence of the Indian Ocean dipole on atmospheric subseasonal variability. *J. Climate,* **18,** 3891–3909.

Sikka, D. R., and S. Gadgil, 1980: On the maximum cloud zone and the ITCZ over Indian longitudes during southwest monsoon. *Mon. Wea. Rev.,* **108,** 1840–1853.

Sprintall, J., A. L. Gordon, R. Murtugudde, and R. D. Susanto, 2000: A semiannual Indian Ocean forced Kelvin wave observed in the Indonesian seas in May 1999. *J. Geophys. Res.,* **105,** 17 217–17 230.

Takayabu, Y. N., T. Iguchi, M. Kachi, A. Shibata, and H. Kanzawa, 1999: Abrupt termination of the 1997–98 El Niño in response to a Madden–Julian oscillation. *Nature,* **402,** 279–282.

Torrence, C., and G. P. Compo, 1998: A practical guide to wavelet analysis. *Bull. Amer. Meteor. Soc.,* **79,** 61–78.

Waliser, D. E., R. Murtugudde, and L. E. Lucas, 2003: Indo-Pacific Ocean response to atmospheric intraseasonal variability. Part I: Austral summer and the Madden–Julian oscillation. *J. Geophys. Res.,* **108,** 3160, doi:10.1029/2002JC001620.

——, ——, and ——, 2004: Indo-Pacific ocean response to atmospheric intraseasonal variability. Part II: Boreal summer and the intraseasonal oscillation. *J. Geophys. Res.,* **109,** 3030, doi:10.1029/2003JC002002.

Wang, B., and H. Rui, 1990: Synoptic climatology of transient tropical intraseasonal convection anomalies: 1975–1985. *Meteor. Atmos. Phys.,* **44,** 43–61.

Webster, P. J., 1983: Mechanisms of monsoon transition: Surface hydrology effects. *J. Atmos. Sci.,* **40,** 2110–2124.

——, A. M. Moore, J. P. Loschnigg, and R. R. Leben, 1999: Coupled ocean–atmosphere dynamics in the Indian Ocean during 1997–1998. *Nature,* **401,** 356–360.

——, and Coauthors, 2002: The JASMINE pilot study. *Bull. Amer. Meteor. Soc.,* **83,** 1603–1630.

Xie, P., and P. A. Arkin, 1996: Analyses of global monthly precipitation using gauge observations, satellite estimates, and numerical model predictions. *J. Climate,* **9,** 840–858.

Yasunari, T., 1981: Structure of an Indian summer monsoon system with around 40-day period. *J. Meteor. Soc. Japan,* **59,** 336–354.

Zhang, Y., W. Rossow, A. Lacis, V. Oinas, and M. Mishchenko, 2004: Calculation of radiative flux profiles from the surface to top-of-atmosphere based on ISCCP and other global datasets: Refinements of the radiative transfer model and the input data. *J. Geophys. Res.,* **109,** D19105, doi:10.1029/2003JD004457.